

High Negative Ion Gain MMThGEM-Micromegas Detector for Directional Dark Matter Searches

A.G. McLean,^{a,b,c,d,1} S. Higashino,^e R.R. Marcelo Gregorio,^{b,d} K. Miuchi,^e and N.J.C. Spooner^d

^a*School of Physics, Chemistry and Earth Sciences, Adelaide University, Adelaide City Campus, Adelaide, SA 5005, Australia*

^b*Department of Nuclear Physics and Accelerator Applications, Australian National University, Garran Road, ACT 2601, Canberra, Australia*

^c*ARC Centre of Excellence for Dark Matter Particle Physics, Australia*

^d*Department of Physics and Astronomy, University of Sheffield, South Yorkshire, S3 7RH, United Kingdom*

^e*Department of Physics, Kobe University, Rokkodaicho, Nada Hyogo 657-8501, Japan*

E-mail: alasdair.mclean@adelaide.edu.au

ABSTRACT: Low pressure gaseous Negative Ion Time Projection Chambers (NITPCs) have been used previously by the DRIFT experiment to search for a directional Dark Matter (DM) signature. The main challenge with using a Negative Ion Drift (NID) gas target is the significantly lower gas gains to which they are typically limited. Recently, a MMThGEM device has been successfully demonstrated as an excellent gain stage device in the NID gas SF₆; capable of producing gas gains comparable with the electron drift gas CF₄. The next major challenge is to extend this high gain capability to multi-dimensional readout for the purpose of particle track reconstruction. The MMThGEM is therefore ideal for coupling to a strip readout detector like a Micromegas to achieve a high gain multi-dimensional Negative Ion (NI) readout plane, which is potentially suitable for the scale up required by future searches proposed by the CYGNUS consortium. In this paper, the first high gain demonstration of such a MMThGEM-Micromegas detector in low pressure SF₆ is described. This includes detector characterisation in a small test vessel resulting in the largest NI gas gain ever reported, $1.22 \pm 0.08 \times 10^5$, and directionality with alpha particles. Finally, this gain characterisation and tracking capability is leveraged to measure the energy and range of events, and identify those consistent with Nuclear Recoils (NRs), in a large cubic metre scale volume of SF₆ for the first time.

KEYWORDS: Dark Matter; WIMP; TPC; MMThGEM; Micromegas; SF₆; Negative Ion; low background experiments.

¹Corresponding author.

Contents

1	Introduction	1
2	Detector Configuration and Experimental Setup	2
3	Effective Detector Gas Gain with ^{55}Fe X-rays	5
4	Directionality with ^{241}Am Alpha Particle Tracks	6
5	^{252}Cf Nuclear Recoils in a CYGNUS-m³ Scale Vessel	8
6	Conclusions	11

1 Introduction

The direct search for Weakly Interacting Massive Particles (WIMPs), potential candidates for the 85% of the Universe’s mass attributed to Dark Matter (DM), has reached the sensitivity limit imposed by the neutrino fog [1–3]. This background now constrains the discovery potential of leading experiments such as LZ, XENONnT, PandaX-4T, and future XLZD detectors. Without precise knowledge of terrestrial neutrino fluxes, these experiments may struggle to deliver conclusive WIMP detection. Directional detection offers a promising alternative for the unambiguous identification of WIMP-like DM [4].

Such a directional search would allow for discrimination between neutrinos, which majoritively originate from the Sun; and WIMPs, which appear to originate from the Cygnus constellation due to the motion of the Solar System through the Milky Way Galaxy. As these origins are separable on Earth at all times, this approach offers the potential for an unimpeded search below the neutrino fog [5]. Furthermore, the galactic origins of this signal would be unambiguous due to its angular modulation caused by the rotation of the Earth on its own axis [6]. In contrast to measurements of annually modulated event rates, this angular modulation could not be conflated with terrestrial sources [7–9]. A directional measurement is therefore considered to be the most conclusive method for WIMP discovery.

Current leading two-phase detector technologies have been found incapable of directional detection [10], therefore an alternative technology is required for this kind of search. Low pressure gaseous Time Projection Chamber (TPC) methods have been used previously, by experiments like DRIFT [11] and NEWAGE [12], to search for directional Nuclear Recoils (NRs) resulting from WIMP interactions. The low pressure allows for longer tracks of ionisation in the gas to better match the spatial resolution of readout technologies. Further to this, the DRIFT experiment conducted a directional WIMP search using the Negative Ion Drift (NID) gas CS_2 for improved reconstruction of events compared to conventional electron drift gases. The use of SF_6 in future searches, like

that proposed by the CYGNUS collaboration [13], is being investigated as an alternative NID gas target. This is because SF₆ is safer to work with and offers improvements in Spin-Dependent (SD) cross-sections with potential WIMP candidates [14]. However, one challenge of using NID gases has always been their limited gas gain resulting in a reduced sensitivity to low energy recoil events.

Recent results with a promising Multi-Mesh Thick Gaseous Electron Multiplier (MMThGEM) device in SF₆ have shown that gas gains in a NID target can be comparable to conventional gases, like CF₄, provided that significant attention is paid to the design and optimisation of the gain stage device [15, 16]. This gain stage device is therefore an ideal candidate for coupling to a strip readout detector like a Micromegas in order to achieve multi-dimensional directionality. In this paper, this coupled detector is introduced, followed by a description of the experimental setup in a test vessel. The effective gas gain is established on the strips and the detector's directional response to alpha particles is evaluated. Finally the response of the detector to NRs is tentatively explored in a large metre cubed scale vessel.

2 Detector Configuration and Experimental Setup

The TPC used in this work is depicted in [Figure 1a](#) and consists of a cathode, a MMThGEM and a Micromegas. A MMThGEM is a MicroPattern Gaseous Detector (MPGD) similar in structure to a Thick-Gaseous Electron Multiplier (ThGEM) [17] which incorporates additional mesh layers [18]. The two stage MMThGEM device, used in this work, consists of top and bottom electrode layers and 4 intermediate mesh layers, for improved amplification properties. These electrode layers establish a collection field, and two pairs of amplification and transfer fields. This design has recently demonstrated significant sub-10⁵ gas gains in SF₆ [15] and has therefore been identified as a suitable gain stage device for coupling with a multi-dimensional readout plane like a Micromegas.

A Micromegas detector is a type of MPGD which utilises a parallel plate avalanche region, established between a mesh electrode and a micro-strip plane [19]. The Micromegas used in this

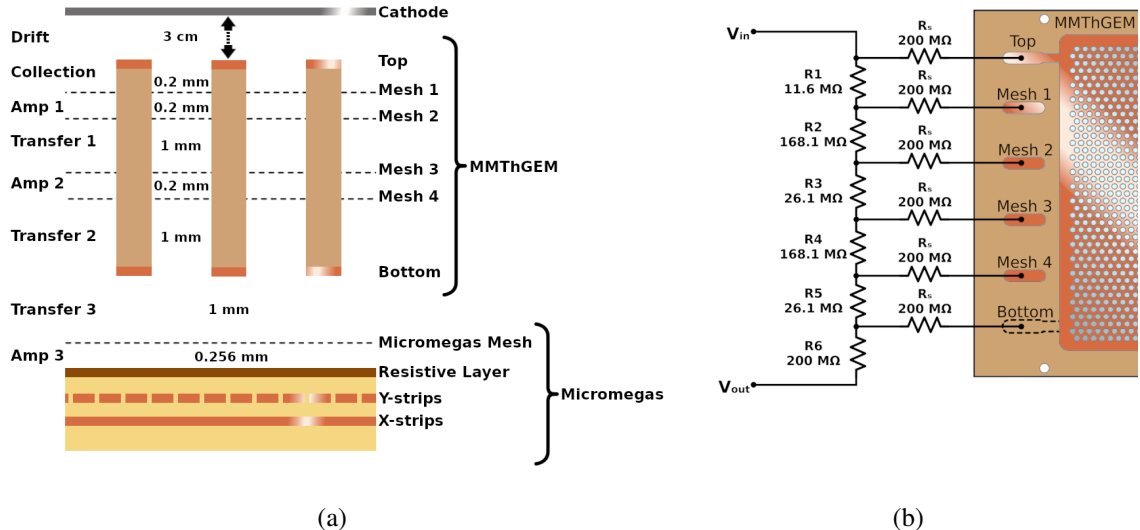


Figure 1: (a) Cross sectional diagram of the coupled MMThGEM-Micromegas detector. (b) Circuit diagram of the MMThGEM resistor chain used for HV biasing.

work was mounted 1 mm below the MMThGEM and consists of a Diamond Like Carbon (DLC) resistive anode layer on top of orthogonal x and y micro-strip electrode planes. The y-strips are situated above the x-strips and have a width of 100 μm and 220 μm respectively with a pitch of 250 μm . The Micromegas has an active area of $10 \times 10 \text{ cm}^2$, identical to the MMThGEM.

For detection to occur in this coupled detector, the charge from ionising events in the drift region is first drifted towards the top of the MMThGEM and then funneled into the holes of the MMThGEM under the influence of the collection field. This charge is then accelerated by the large field strength of the first amplification field resulting in a cascade of ionisation which serves to amplify the charge. This amplified charge is transferred to the second amplification field, by a smaller transfer field strength, where it is accelerated and amplified for a second time. The charge is then transferred towards the Micromegas by the second and third transfer fields before being amplified again by the third and final amplification field in the Micromegas. Finally, the amplified charge is measured on 32 Micromegas y-strips instrumented with LTARS2018 charge sensitive electronics [20]. This amounts to a total instrumented area of 7.85 mm \times 10 cm.

The MMThGEM biasing was handled by two HV supplies and a resistor chain soldered to the biasing connections, shown in Figure 1b. These resistor values were derived from a previous optimisation in 40 Torr SF₆ [15]. Two additional HV supplies were used for biasing the cathode and micromegas mesh separately, while the resistive layer and strips of the micromegas were connected to ground. All four HV channels were provided by CAEN A7030DP and A7030DN modules.

For detector characterisation, the MMThGEM-Micromegas TPC was assembled and mounted at the centre of an aluminium plate (Figure 2a), which was attached to the door of a small test vessel. The detector assembly was then sealed inside the vessel which also featured a thin kapton window, shown in Figure 2b, to aid exposure to radioactive sources. The test vessel was evacuated and filled

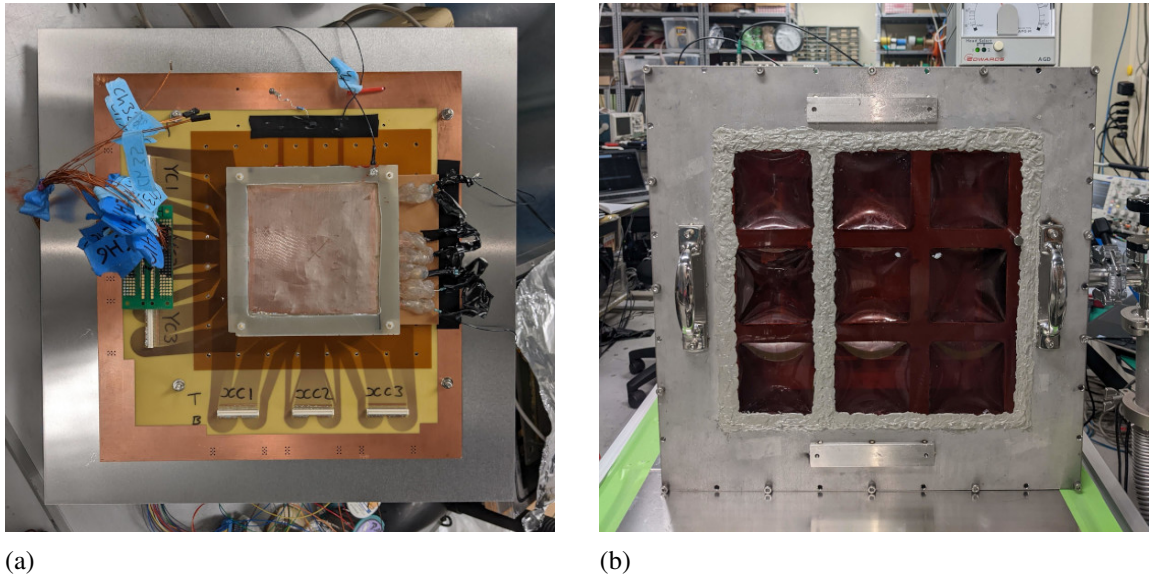


Figure 2: (a) Image of the coupled MMThGEM-Micromegas TPC assembly mounted to the door of the test vessel. (b) Image of the test vessel with brown kapton window containing the coupled MMThGEM-Micromegas TPC assembly mounted inside.

with 40 Torr of SF₆ and sources of ionising radiation were positioned around the instrumented TPC volume. The sources included an ⁵⁵Fe X-ray source (Section 3), 0.8 MBq, and an ²⁴¹Am alpha particle source (Section 4), $O(10)$ kBq. A diagram was created to illustrate the source positions relative to the instrumented TPC volume and can be seen in Figure 3.

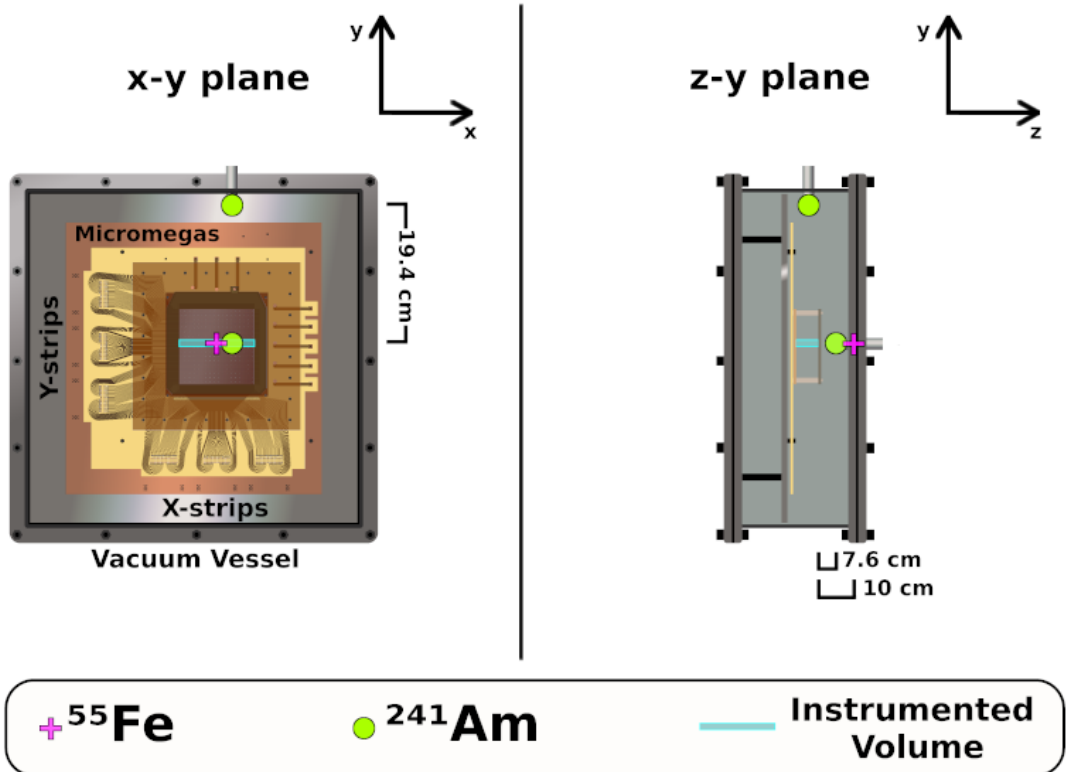


Figure 3: Diagram of small test vessel showing the positioning of radioactive sources around the TPC volume.

The panel on the left of Figure 3 shows a cross section of the test vessel in the x-y plane, while the panel on the right shows the z-y plane. The cross section of the instrumented TPC volume can be seen highlighted in cyan above the micromegas plane. The source positions can be seen indicated by a magenta plus and green circle icons for the ⁵⁵Fe and ²⁴¹Am positions respectively. During the X-ray exposure, the ⁵⁵Fe source was positioned externally in the kapton window of the test vessel with an offset in the z-dimension of 10 cm from the instrumented volume. For the purpose of orthogonal directional measurements, the ²⁴¹Am source was given a y-axis and z-axis exposure position. During the y-axis exposure, the ²⁴¹Am source was positioned internally with a 19.4 cm distance in the y-dimension from the instrumented volume. During the z-axis exposures, it can be seen that the ²⁴¹Am source was positioned directly in front of the instrumented volume with a separation in the z-axis of 7.6 cm.

3 Effective Detector Gas Gain with ^{55}Fe X-rays

The effective gas gain of the detector is required to determine the electron equivalent energy of events, in this section the gas gain is determined with the ^{55}Fe source. X-ray events were successfully detected on the micromegas strips with HV biasing of -2900 V, -1900 V, 100 V, and -530 V for the cathode, V_{in} , V_{out} and micromegas mesh respectively. Due to the MMThGEM hole size and charge dissipation in the resistive layer, events span across several strips. Therefore, a cut was applied to ensure that the charge was not artificially diminished by falling outside the instrumented area. Events were cut if the central channel number was less than 13 or more than 18. Events passing this cut were binned according to the signal integral, converted to charge via a calibration performed by capacitive charge injection, and summation across all 32 strips. The resulting spectrum is shown in [Figure 4](#).

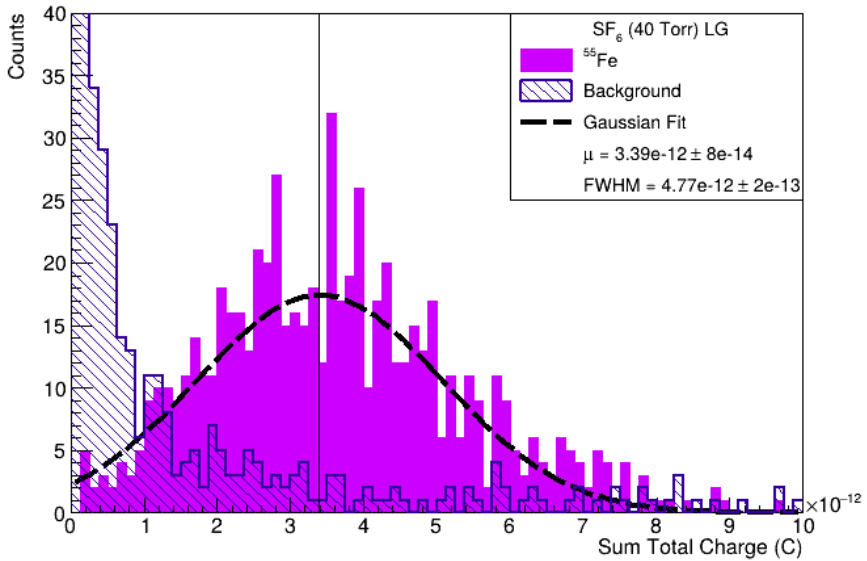


Figure 4: Sum total charge spectrum with the signal integral method as measured on the LG channels.

The ^{55}Fe spectrum is shown in solid magenta along with a background exposure in hatched violet. A Gaussian function was fit to the ^{55}Fe exposure data and can be seen as a dashed black line with the mean of the Gaussian indicated by a vertical black line. The gain was determined via the ^{55}Fe X-ray energy, 5.89 keV, and W-value of SF₆, 34 eV [21]. It was found that the detector produced an effective gas gain of $1.22 \pm 0.08 \times 10^5$ with an energy resolution of 1.41 ± 0.07 . The energy resolution is calculated as the FWHM (Full Width at Half Maximum) of the Gaussian divided by the mean.

This result is a significant ancillary benefit of the detector coupling because this is the first time a gas gain on the order of 10^5 has been achieved with an NID gas; furthermore, this is more than two orders of magnitude larger than typical NID gas gains. This result is credible considering that the MMThGEM is known to be providing an amplification factor of $\approx 10^4$ [15] and the micromegas mesh provides additional amplification; an apparent amplification factor ≈ 12.2 .

4 Directionality with ^{241}Am Alpha Particle Tracks

Determining the principle axis of particle tracks and identifying sense via $\frac{dE}{dx}$ signatures is important for directional searches. In this section, work in which a 2-dimentional track reconstruction algorithm was developed, and tested via exposures to an ^{241}Am alpha particle source, is presented. Due to the highly ionising nature of alpha particles, the field strengths were lowered during these runs to reduce sparking. The voltages applied to the cathode, V_{in} , V_{out} , and the micromegas mesh were -2800 V, -1800 V, 100 V, and -500 V respectively.

Alpha tracks were successfully detected in both the z-axis and y-axis exposure directions, outlined in [Section 2](#), examples of which can be seen in [Figure 5](#). The channel number is plotted against time, where the instantaneous voltage of each channel is indicated by the colour scale in mV, and the points above a 40 mV threshold are indicated by magenta markers. During the z-axis alpha particle exposure, events were observed to have discontinuity between consecutive charge clusters, shown on the left of [Figure 5](#). This was found to be caused by the MMThGEM hole pitch because the cluster separation was consistent with the 1.2 mm hole pitch.

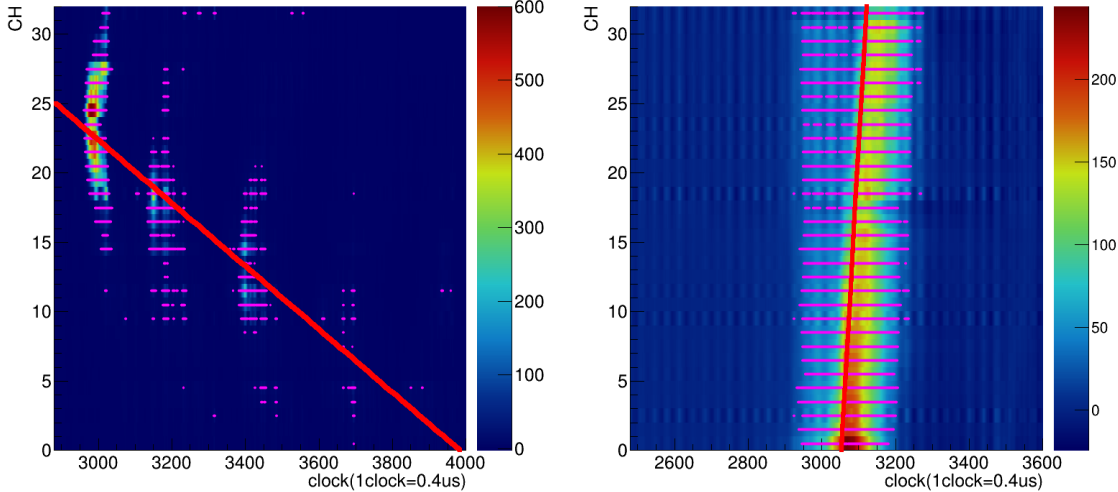


Figure 5: An example z-axis exposure event (left) and y-axis exposure event (right). Points above a 40 mV threshold are indicated by magenta markers and the TLR fit is indicated by a red line.

A Total Linear Regression (TLR), also known as Deming regression, algorithm was developed for determining the principle axis of alpha tracks in the y-axis and z-axis exposures; this accounts for the residuals in both axes and effectively handles the highly rectilinear nature of alpha particle tracks. This algorithm was implemented by first determining all the points above a 40 mV threshold, followed by the conversion of these coordinates to spatial units via the micromegas strip pitch and ion drift velocity. For each event, the gradient, m , and y-intercept, c , of the track in the z-y plane was calculated as [22]:

$$m = -p + \sqrt{1 + p^2}, \quad c = \bar{Y} - m\bar{Z}, \quad \text{where} \quad p = \frac{S_{ZZ} - S_{YY}}{S_{ZY}},$$

\bar{Y} and \bar{Z} are the average y and z coordinates of those above threshold and S_{ZZ} , S_{YY} , and S_{ZY} are defined as:

$$S_{ZZ} = \frac{1}{n} \sum_{i=1}^n Z_i^2 - \bar{Z}, \quad S_{YY} = \frac{1}{n} \sum_{i=1}^n Y_i^2 - \bar{Y}, \quad S_{ZY} = \frac{1}{n} \sum_{i=1}^n Z_i Y_i - \bar{Z} \bar{Y}, \quad (4.1)$$

where n is the total number of points above threshold. By visual inspection, the algorithm performed well for track reconstruction during both perpendicular exposures. The result of this algorithm applied to a z-axis and y-axis exposure event can be seen overlaid in red in [Figure 5](#).

The TLR algorithm was applied to all events in the z-axis and y-axis exposures and θ , the angle between the z-axis and the reconstructed track, was calculated. The results of which, shown in [Figure 6](#), display clear angular separation between events from the two orthogonal exposures. The z-axis events peak at $\theta = 0^\circ$ while the y-axis events peak at $\theta = 90^\circ$. This result highlights the effectiveness of the TLR algorithm for accurately determining the principle axis in 2-dimensions.

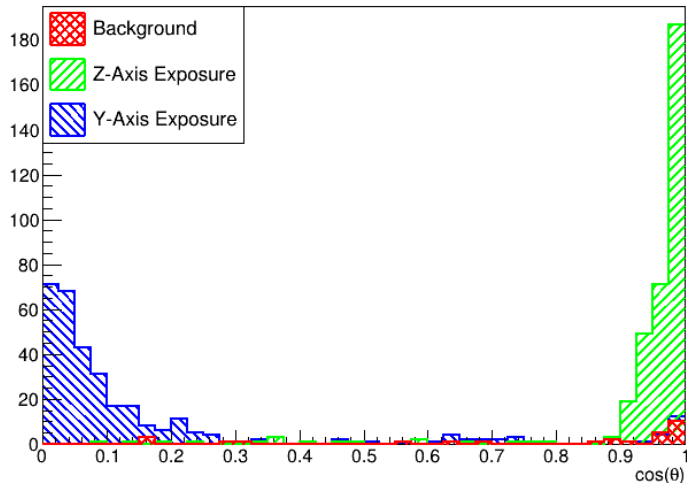


Figure 6: Distribution of the angle between the principle axis of an event and the z-axis determined via the TLR algorithm.

Furthermore, the $\frac{dE}{dx}$ signatures of the alpha tracks in [Figure 5](#) are consistent with simulated events. A SRIM (Stopping and Range of Ions in Matter) [23] simulation of 5.5 MeV alpha particles in 40 Torr of SF₆ was performed and the regions of interest for both the z-axis and y-axis exposures can be seen on the right of [Figure 7](#), highlighted in green and blue respectively. The intensity of the charge clusters in the z-axis exposure event increases from right to left, in the direction of the alpha particles motion. While the intensity of the measured charge in the y-axis exposure event decreases along the length of the track; the alpha particle is travelling from channel 0 to 31. This result is significant because it demonstrates that charge asymmetries, and therefore directional sense, can be resolved with this detector.

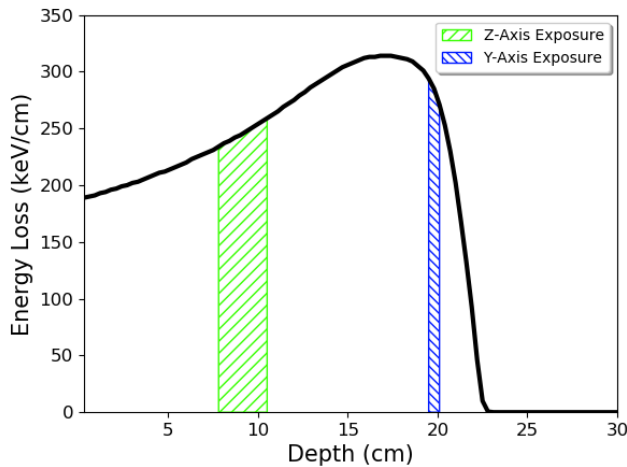


Figure 7: Bragg curve simulated with 10,000 5.5 MeV alpha particles in 40 Torr of SF₆ using SRIM. Hatched areas indicate the section measured by the instrumented strips.

5 ^{252}Cf Nuclear Recoils in a CYGNUS-m³ Scale Vessel

Following the successful characterisation and initial receptiveness to a ^{252}Cf neutron source, the MMThGEM-Micromegas detector was transferred from the test vessel to the Kobe University C/N-1.0 vessel to enable the measurement of NRs in a full-scale detector volume of low-pressure SF₆. The C/N-1.0 vessel, shown on the left of Figure 8, is a CYGNUS-m³ scale vessel [13] with back-to-back 1.6 m x 1.6 m x 0.5 m volumes. It can accommodate up to 18 small R&D readout planes mounted on nine panels per side. The MMThGEM-Micromegas was installed centrally via the panel-compatible vessel door assembly.

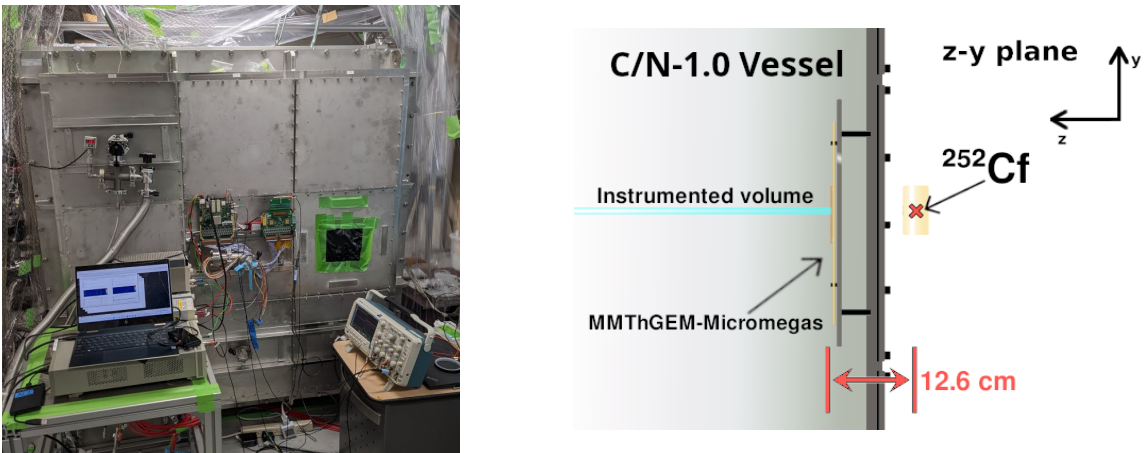


Figure 8: Image of the C/N-1.0 vessel following installation of the detector panel (left). Cross sectional diagram depicting the ^{252}Cf neutron source position relative to the MMThGEM-Micromegas assembly in the C/N-1.0 vessel (right).

After installation, the C/N-1.0 vessel was evacuated and filled with 40 Torr of SF₆; this marks the first instance in which such a large volume of low pressure SF₆ has been utilised. Once filled, V_{in}, V_{out} and the micromegas mesh voltages were once again set to -1900 V, 100 V, and -530 V while the cathode was set to -18.55 kV; to replicate the field strengths used in [Section 3](#). The ²⁵²Cf source was then placed externally in front of the central panel with a z-axis offset of 12.6 cm from the instrumented TPC volume, as illustrated on the right of [Figure 8](#).

Events were acquired over the course of 13 hours and 1210 events were successfully captured. Two notable example events from the exposure can be seen in [Figure 9](#). The successful observation of events in such a large volume of low pressure SF₆ is a significant step forward for demonstrating the MMThGEM-Micromegas detector as a scalable readout technology for a future CYGNUS search.

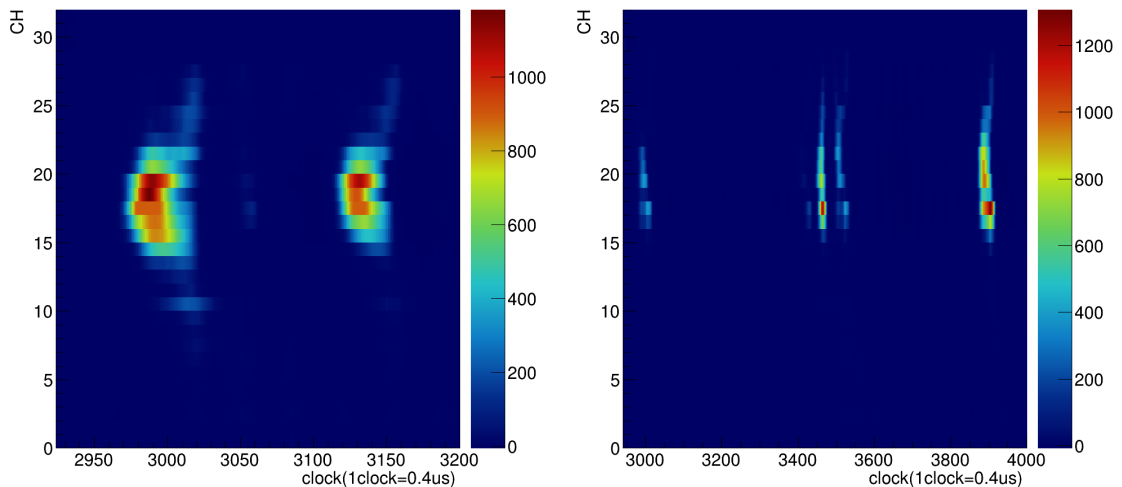


Figure 9: Examples of events which were captured during the ²⁵²Cf neutron source exposure in the C/N-1.0 vessel.

The event on the left of [Figure 9](#) consists of two symmetric clusters of charge, likely caused by the charge discontinuity effect discussed previously in [Section 4](#). Interestingly, this particular event exhibits some preliminary evidence of the head-tail effect, with neutrons incident from the left-hand side. The event on the right of [Figure 9](#) contains four charge clusters. This could be caused purely by the charge discontinuity effect, or it could be an indication of two SF₅⁻ minority peaks. In the latter case, the charge in the smaller leading clusters contain $\sim 30\%$ of that in the larger respective trailing clusters, much larger than those seen previously at lower gas gains [[14](#)]. This could suggest that the large gain of this detector constitutes a significant sensitivity increase to measurable minority peaks. These results are greatly promising for this detector and further work is required to investigate sensitivity to the head-tail effect and minority peaks in the future.

The recoil energies of measured events during the neutron run in the C/N-1.0 vessel were calculated by first converting the signal integral into charge, via the calibration, and then relating this measured charge to the initial amount of ionisation charge via the gas gain, determined in [Section 3](#). Finally this was related to the amount of electron equivalent energy via the SF₆ W-value.

The 2-dimensional recoil range was then calculated by first determining the z-range from the points above a 40 mV threshold. The y-range was then determined via the TLR algorithm, described in [Section 4](#), to minimise the influence of charge dissipation in the resistive layer. The resulting 2-dimensional range of each event can be seen plotted against the estimated recoil energy in [Figure 10](#); indicated by the black cross markers.

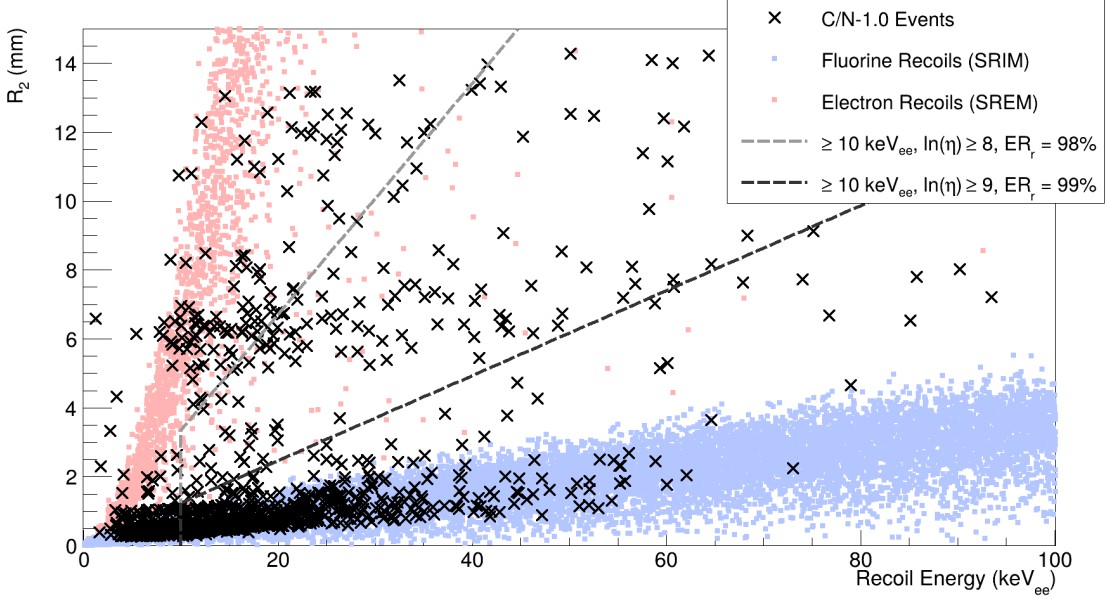


Figure 10: Two-dimensional range vs estimated recoil energy for events observed in the C/N-1.0 vessel during the ^{252}Cf neutron exposure (black cross markers). The simulated NR and ER events from SRIM (pale blue) and SREM (pale red) are also observed along with the selection cuts described in the previous subsection.

Supplementary SRIM and SREM simulations of NRs and ERs respectively are also shown in [Figure 10](#). Given the relative abundance of fluorine in SF_6 , the recoil of 100 fluorine nuclei were simulated for every 1 keV increment between 1 and 150 keV in 40 Torr of SF_6 (pale blue); the energy was converted to keV_{ee} via the Lindhard model [24, 25]. SREM was then used in a similar fashion to simulate 100 ERs for each 1 keV increment between 1 and 100 keV (pale red). A parameter was defined to facilitate a $\frac{dE}{dx}$ cut such that:

$$\eta = E/R_2,$$

where E is the electron equivalent energy in keV_{ee} and R_2 is the 2-dimensional range in the z-y plane in metres. This is analogous to a parameter whose natural logarithm has previously been used for ER/NR discrimination in low pressure CF_4 [26] and SF_6 [27]. Using the simulated data, a strict cut which included events above 10 keV_{ee} with $\ln(\eta) \geq 9$ and a more lenient cut with $\ln(\eta) \geq 8$ were made; with ER rejection of 99% and 98% respectively.

As shown in [Figure 10](#), a significant portion of C/N-1.0 events appear to strongly correlate with the simulated NR band and fall well within the $\text{ER}_r = 99\%$ selection cut, indicating that a large portion of events are consistent with NRs. A number of events can also be seen to cluster

close to the simulated ER band and fall outside the $ER_r = 98\%$ selection cut, suggesting that these events are consistent with ERs. Events can also be seen to fall between the two selection cuts and are neither consistent with the NR or ER band. Some of these could be a consequence of mishandling events which contain minority peaks or are not constrained to the instrumented area as well as diffusion and charge dissipation effects. Therefore, further work is required to investigate these events. This would include scaling up the number of instrumented channels in both x and y-strip planes for complete 3-dimensional event reconstruction, as well as exposure to a high energy gamma-ray source for a more explicit ER/NR discrimination study.

Figure 11 presents a more focused view of the distribution of the measured recoil ranges (left) and energies (right) from the C/N-1.0 vessel. With no selection cuts applied, events appear to accumulate in three distinct clusters in the range distribution. Upon inspection, this was found to be a quantisation artefact induced by the coarse MMThGEM hole pitch, discussed in Section 4. This structure is not present following the strict selection cut, most likely due to the short (< 4 mm) range of NRs in this energy range. Finally, it is noted that the measured energy spectrum is consistent with that of a ^{252}Cf neutron source demonstrated elsewhere in similar low pressure gaseous detector exposures [26, 28]. These findings provide strong evidence that NRs were successfully observed during operation in the large C/N-1.0 vessel. This result therefore represents a significant step towards realising this detector technology as a scalable readout option for a CYGNUS search.

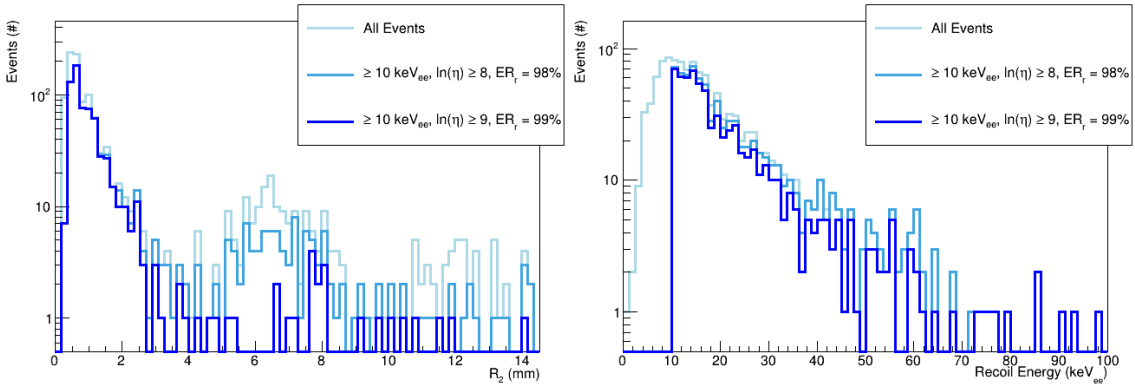


Figure 11: Histograms showing the measured ranges (left) and energies (right) of all recoil events (pale blue) and with the lenient (light blue) and strict (blue) simulated selection cuts applied.

6 Conclusions

In conclusion, the operation of a coupled MMThGEM-Micromegas detector in low pressure SF_6 was discussed in this paper. 32 y-strips were individually instrumented, demonstrating the largest area of individually instrumented strips in an NID gas with this detector to date. This was made possible by the large gas gain of $1.22 \pm 0.08 \times 10^5$. This is an improvement on the previous measurements with the isolated MMThGEM and demonstrates the first charge amplification of order 10^5 in an NID gas; two orders of magnitude larger than typical NID gas gains previously seen. Complete 2-dimensional directionality was also demonstrated with alpha particle tracks by

reconstruction of the principle axis, through development of a total linear regression algorithm; and by sense recognition, where $\frac{dE}{dx}$ signatures were found to be consistent with simulated alpha tracks. Following characterisation in the test vessel, the detector was installed in the CYGNUS-m³ scale C/N-1.0 vessel and exposed to a ²⁵²Cf neutron source, with most observed events found to be consistent with simulated fluorine nuclear recoils. While further work is required for explicit ER/NR discrimination, head-tail sensitivity, and minority peak observations, these results represent an important step toward scaling this technology for a CYGNUS search. It is recommended for future designs to reduce MMThGEM hole pitch and remove the micromegas resistive layer to mitigate track discontinuity and charge dissipation effects.

Acknowledgments

The authors would like to acknowledge the "University of Sheffield EPSRC Doctoral Training Partnership (DTP) Case Conversion Scholarship" awarded to A.G. McLean. This work was also partially supported by the Japanese Ministry of Education, Culture, Sports, Science and Technology, Grant-in-Aid (24K07061 and 25K01025).

References

- [1] Z. Bo et al., Phys. Rev. Lett. 133 (2024) 191001
- [2] E. Aprile et al., Phys. Rev. Lett. 133 (2024) 191002
- [3] D. S. Akerib et al., arXiv:2512.08065 (2025)
- [4] C. A. J. O'Hare, Phys. Rev. Lett. 127 (2021) 251802
- [5] S. E. Vahsen et al., Annu. Rev. Nucl. Part. Sci. 71 (2012) 189
- [6] B. Morgan, Nucl. Instrum. Methods. Phys. Res. A. 513 (2003) 226
- [7] J. Klinger and V. A. Kudryavtsev., Phys. Rev. Lett. 114 (2015) 151301
- [8] V. A. Kudryavtsev et al., J. Phys.: Conf. Ser. 203 (2010) 012039
- [9] J. H. Davis Phys. Rev. Lett. 113 (2014) 081302
- [10] DarkSide-20k Collaboration., Eur. Phys. J. C. 84 (2024) 24
- [11] J. B. R. Battat et al., Astropart. Phys. 91 (2017) 65
- [12] T. Shimada et al., Prog. Theor. Exp. Phys. 10 (2023) 103F01
- [13] S. E. Vahsen et al., arXiv:2008.12587 (2020)
- [14] N. S. Phan et al., JINST 12 (2017) P02012
- [15] A.G. McLean et al. JINST 19 (2024) P03001
- [16] F. D. Amaro et al., JINST 19 (2024) P06021
- [17] S. Bressler et al., Prog. Part. Nucl. Phys. 130 (2023) 104029
- [18] R. de Olivera and M. Cortesi, JINST 13 (2018) P06019
- [19] D. Attie et al., Appl. Sci. 11 (2021) 5362
- [20] T. Kosaka et al., J. Phys. 2374 (2022) 012077

- [21] I. Lopes et al., *J. Phys. D.* 19 (1986) 107
- [22] P. Glaister, *Math. Gaz.* 85 (2001) 104
- [23] P. Hovington and D. Drouin, "The Stopping and Range of Electrons in Matter" (2024)
<http://www.srim.org/SREM.htm>
- [24] J. Lindhard et al., *Mat. Fys. Medd. Dan . Vid. Selsk .* 33 (1963) 10
- [25] P. Sorensen, *Phys. Rev. D.* 91 (2015) 083509
- [26] N. S. Phan et al., *Astropart. Phys.* 84 (2016) 82
- [27] R. J. Lafler, Thesis, University of New Mexico. (2019)
- [28] C. Eldridge, Thesis, University of Sheffield. (2021)